Letters

Low-Frequency Stability Analysis of Train-Grid System: A Perspective From DAB Converter

Chunxu Lin, *Student Member, IEEE*, Xinglai Ge, *Senior Member, IEEE*, Huimin Wang, *Member, IEEE*, Xiangyu Meng, *Graduate Student Member, IEEE*, Junwen Mu, *Student Member, IEEE*, and Zhigang Liu, *Fellow, IEEE*

***Abstract*—Despite the great potential of power electronic traction transformer (PETT) in high-speed train, the issue of low-frequency oscillation (LFO) is a concern. Unfortunately, current studies assessing the low-frequency stability of the PETT often oversimplify the dual active bridge (DAB) converter as a passive circuit, which may lead to an unreliable analysis result. To clarify this issue, this letter examines the mechanism of LFO in the PETT-based train-grid system from the perspective of a DAB converter. Specifically, a complete impedance model of the PETT is first established by using the harmonic linearization method. Then, the stability differences between simplified PETT and complete PETT are investigated, and the impact mechanism of DAB converter on the LFO is thoroughly revealed. The experimental test results verify the correctness of modeling and analysis.**

***Index Terms*—Dual active bridge (DAB) converter, harmonic linearization modeling, low-frequency oscillation (LFO) analysis, power electronic traction transformer (PETT).**

I. Introduction

In the high-speed train, substituting the line frequency transformer, the power electronic traction transformer (PETT) consisting of cascaded H-bridge (CHB) rectifiers and dual active bridge (DAB) converters is promising to improve the efficiency and reduce the weight [1], [2]. Despite this, the PETT is burdened by some stability issues due to complex interactions between the PETT-based train and the traction grid. One of the major concerns for the stable operation of PETT is referred to as the issue of low-frequency oscillation (LFO) [3].

To explore the issue of LFO in the PETT, a double-input double-output model is established in [3], where the dc–dc converter is equated to an *RC* circuit for simplifying analysis. With this, the impacts of control parameters on the LFO are investigated. Additionally, a simplified *dq*-frame model is developed in [4] to analyze the harmonic stability of the PETT-based train-grid system, in which the DAB converter is equivalent to an *RLC* load. A small-signal model of power electronic transformer that neglects some dynamics of the ac–dc converter is established in [5] to assess the stability of the cascaded system. Moreover, an equivalent multiport circuit of the PETT is presented in [6] to conduct the current and power analysis. Notice that the PETT contains a two-stage structure, but the above works often establish a simplified model for analysis and control. Especially in terms of stability analysis of the PETT, the impact of the DAB converter is negligible and it is often replaced by a passive circuit. In experimental testing, however, it is found that the low-frequency stability of the PETT-based train-grid system is sensitive to the DAB converter, which is hardly reported in current studies. Hence, the influence of the DAB converter on the LFO of PETT-based train-grid system is not been fully revealed. Due to this, the accuracy of stability analysis may be limited, resulting in an overly optimistic result in practical PETT applications.

Motivated by the above discussion, this letter presents a new perspective for analyzing the low-frequency stability of the PETT-based train-grid system. The main contributions are introduced as follows.

1) A comprehensive impedance model of the PETT is first developed by using the harmonic linearization method, which is able to improve the accuracy of stability analysis.
2) A novel analysis method based on the DAB converter perspective is proposed, and the mechanism of how the DAB converter affects the LFO of the PETT-based train-grid system is thoroughly revealed.

II. Harmonic Linearization Modeling of the PETT

The topology and control strategy of the PETT are given in Fig. 1, which consists of N identical cells. In each cell of PETT, u_1, i_1, and C_1 are the dc-link voltage, current, and capacitor of the rectifier, respectively. u_2, i_2, and C_2 are the output voltage, current, and capacitor of the DAB converter. L_r is the equivalent

Manuscript received 9 January 2024; revised 23 February 2024; accepted 25 March 2024. Date of publication 8 April 2024; date of current version 20 June 2024. This work was supported by Sichuan Science and Technology Program under Grant MZGC20230015. *(Corresponding author: Huimin Wang.)*

Chunxu Lin, Xinglai Ge, Huimin Wang, and Junwen Mu are with the Ministry of Education Key Laboratory of Magnetic Suspension Technology and Maglev Vehicle, Southwest Jiaotong University, Chengdu 610031, China (e-mail: lincx@my.swjtu.edu.cn; xlge@swjtu.edu.cn; wanghuimin@my.swjtu.edu.cn; mujunwen@my.swjtu.edu.cn).

Xiangyu Meng and Zhigang Liu are with the School of Electrical Engineering, Southwest Jiaotong University, Chengdu 611756, China (e-mail: mengxy55@126.com; liuzg_cd@126.com).

Color versions of one or more figures in this article are available at https://doi.org/10.1109/TPEL.2024.3386360.

Digital Object Identifier 10.1109/TPEL.2024.3386360

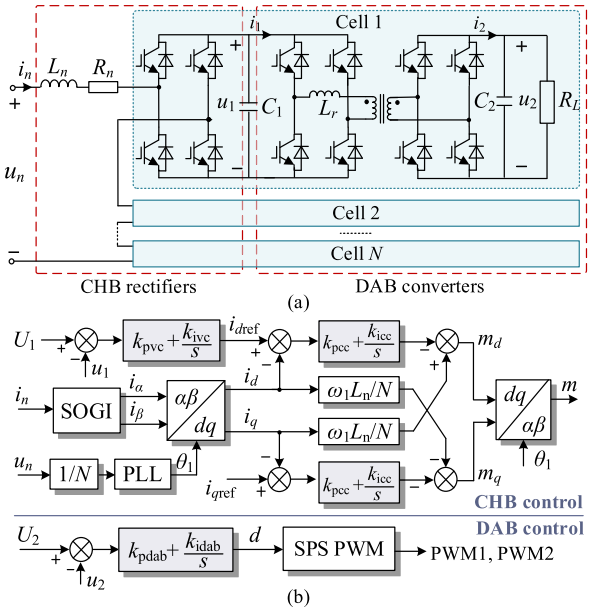

Fig. 1. Block diagram of PETT. (a) Topology. (b) Main control strategies.

leakage inductance of isolation transformer, and R_L is the power load. For the DAB converter with a single-phase-shift control [6], the average transmitted power is described as

$$P = U_1 U_2 D(1-D)/2nf_s L_r \tag{1}$$

where U_1, U_2, D, n, and f_s are the reference values of u_1 and u_2, the phase-shift ratio, the transformer ratio, and the switching frequency of DAB converter, respectively. Based on the small-signal perturbation method, the input and output currents of DAB converter are described as

$$\begin{cases} \hat{i}_1 = \frac{U_2(1-2D)}{2nf_s L_r}\hat{d} + \frac{D(1-D)}{2nf_s L_r}\hat{u}_2 = G_{1d}\hat{d} + G_{1u}\hat{u}_2 \\ \hat{i}_2 = \frac{U_1(1-2D)}{2nf_s L_r}\hat{d} + \frac{D(1-D)}{2nf_s L_r}\hat{u}_1 = G_{2d}\hat{d} + G_{2u}\hat{u}_1 \end{cases} \tag{2}$$

where the superscript "^" represents small-signal expressions of the corresponding variables. For the load circuit of the DAB converter, the small-signal equation can be written as

$$\hat{u}_2 = \hat{i}_2 \cdot Z_L = Z_L G_{2d} \cdot \hat{d} + Z_L G_{2u} \cdot \hat{u}_1 \tag{3}$$

with $Z_L = R_L/(1+sC_2R_L)$. Based on the control strategy of the DAB converter, as shown in Fig. 1, it meets

$$\hat{d} = -\left(k_{\text{pdab}} + k_{\text{idab}}/s\right)\hat{u}_2 = G_{uc}\hat{u}_2 \tag{4}$$

where k_{pdab} and k_{idab} are the control gains of the proportional integral (PI) controller. Then, the impedance of the DAB converter is deduced as follows by substituting (3) and (4) into (2)

$$Z_{\text{dab}} = \frac{\hat{u}_1}{\hat{i}_1} = \frac{1 - Z_L G_{2d} G_{uc}}{(G_{1d}G_{uc} + G_{1u})Z_L G_{2u}}. \tag{5}$$

Thus, in a cell of the PETT, the load of rectifier is denoted by $Y_d = sC_1 + 1/Z_{\text{dab}}$. Then, the main circuit of PETT is expressed as

$$\begin{cases} L_n \frac{di_n}{dt} = u_n - R_n i_n - N m u_{\text{dc}} \\ m i_n = Y_d u_{\text{dc}} \end{cases} \tag{6}$$

where L_n, R_n, i_n, and m are the ac-side inductance and its resistance, the ac-side current, and the modulation signal of CHB rectifiers [7], respectively.

The harmonic linearization-based impedance modeling approach is attractive due to its advantage of easy measurement. Thus, with a small sinusoidal perturbation, the frequency-domain expressions of u_n, i_n, and m are expressed as

$$\hat{\boldsymbol{u}}_{\mathbf{n}} = [0, \dot{U}_p, 0]^{\mathrm{T}},\ \hat{\boldsymbol{i}}_{\mathbf{n}} = [0, \dot{I}_p, 0]^{\mathrm{T}},\ \hat{\boldsymbol{u}}_{\mathbf{1}} = [\dot{U}_{1-}, 0, \dot{U}_{1+}]^{\mathrm{T}} \tag{7}$$

where the frequency element is $f = [f_p - f_1, f_p, f_p + f_1]^{\mathrm{T}}$ (f_p is the disturbance frequency and f_1 is the fundamental frequency), and $\dot{U}_p$, $\dot{I}_p$, $\dot{U}_{1-}$, and $\dot{U}_{1+}$ are the corresponding phasors. Hence, based on the harmonic balance principle, (6) is modified as

$$\begin{cases} \hat{\boldsymbol{u}}_{\mathbf{n}} - \boldsymbol{Z}_{\mathbf{n}}\hat{\boldsymbol{i}}_{\mathbf{n}} = \boldsymbol{U}_{\mathbf{1}}\hat{\boldsymbol{m}} + \boldsymbol{M}\hat{\boldsymbol{u}}_{\mathbf{1}} \\ \boldsymbol{I}_{\mathbf{n}}\hat{\boldsymbol{m}} + \boldsymbol{M}\hat{\boldsymbol{i}}_{\mathbf{n}} = \boldsymbol{Y}_{\mathbf{d}}\hat{\boldsymbol{u}}_{\mathbf{1}} \end{cases} \tag{8}$$

where $\boldsymbol{M}$, $\boldsymbol{U_1}$, and $\boldsymbol{I_n}$ are the Toeplitz matrix expressions for the steady-state vectors of variables m, u_{dc}, and i_n. Moreover, $\boldsymbol{Z_n}$ and $\boldsymbol{Y_d}$ are the diagonal matrix, i.e., $\boldsymbol{Z_n} = \text{diag}[Z_n(s_{-1}), Z_n(s), Z_n(s_{+1})]$ and $\boldsymbol{Y_d} = \text{diag}[Y_d(s_{-1}), Y_d(s), Y_d(s_{+1})]$, with the symbol $s_{\pm 1}$ meaning frequency shift $s \pm j\omega_1$.

In the control strategy of the CHB rectifiers, a second-order generalized integrator (SOGI) is used to generate the quadrature signal. Then, through the Park transformation, the dq-frame currents are expressed as

$$\begin{cases} \hat{\boldsymbol{i}}_{\mathbf{d}} = 0.5\dot{I}_p[H_\alpha(s_{+1}) + jH_\beta(s_{+1}), 0, H_\alpha(s_{-1}) - jH_\beta(s_{-1})]^{\mathrm{T}} \\ \hat{\boldsymbol{i}}_{\mathbf{q}} = 0.5\dot{I}_p[H_\beta(s_{+1}) - jH_\alpha(s_{+1}), 0, jH_\alpha(s_{-1}) + H_\beta(s_{-1})]^{\mathrm{T}} \end{cases} \tag{9}$$

where $H_\alpha(s)$ and $H_\beta(s)$ are the transfer functions of the SOGI [4].

The output of dc-link voltage controller is the reference value of the active current. Thereby, the expression of i_{dref} is given as follows:

$$\hat{\boldsymbol{i}}_{\mathbf{dref}} = \left[-H_{\text{vc}}(s)\dot{U}_{1-}, 0, -H_{\text{vc}}(s)\dot{U}_{1+}\right]^{\mathrm{T}} \tag{10}$$

where $H_{\text{vc}}(s) = k_{\text{pvc}} + k_{\text{ivc}}/s$. k_{pvc} and k_{ivc} are the proportional and integral parameters of the dc-link voltage controller.

Based on the CHB control shown in Fig. 1, the dq-frame modulation signals are given by

$$\begin{cases} m_d = -(i_{\text{dref}} - i_d)H_{\text{cc}}(s) + K_{ou} i_q \\ m_q = -H_{\text{cc}}(i_{\text{qref}} - i_q) - K_{ou} i_d \end{cases} \tag{11}$$

where $K_{ou} = \omega_1 L_n/N$ and $H_{\text{cc}}(s) = k_{\text{pcc}} + k_{\text{icc}}/s$. k_{pcc} and k_{icc} are the proportional and integral parameters of the current controller. Correspondingly, the small-signal expressions of modulation signals are written as follows:

$$\begin{cases} \hat{\boldsymbol{m}}_{\mathbf{d}} = \left[H_{\text{co}}(s)\dot{U}_{1-} + 0.5k_{m1}(s)\dot{I}_p, 0, H_{\text{co}}(s)\dot{U}_{1+}\right. \\ \quad \left. + 0.5k_{m2}(s)\dot{I}_p\right]^{\mathrm{T}} \\ \hat{\boldsymbol{m}}_{\mathbf{q}} = \left[0.5k_{m3}(s)\dot{I}_p, 0, 0.5k_{m4}(s)\dot{I}_p\right]^{\mathrm{T}} \end{cases} \tag{12}$$

where $H_{co}(s) = H_{vc}(s) \cdot H_{cc}(s)$, and $k_{m1}(s)$–$k_{m4}(s)$ are the conversion coefficient, presented in the Appendix.

Thus, the small-signal expression of m is further derived as follows:

$$\hat{\boldsymbol{m}} = \boldsymbol{Q_1}\hat{\boldsymbol{u}}_1 + \boldsymbol{Q_2}\hat{\boldsymbol{i}}_\mathbf{n} \tag{13}$$

where $\boldsymbol{Q_1}$ and $\boldsymbol{Q_2}$ are the transfer function matrices, and they are shown in the Appendix. Substituting (13) into (8), it yields

$$\boldsymbol{Z_t} = \boldsymbol{Z_n} + \boldsymbol{U}_1\boldsymbol{Q_2} + (\boldsymbol{U}_1\boldsymbol{Q_1} + \boldsymbol{M}) \cdot (\boldsymbol{Y_d} - \boldsymbol{I_n}\boldsymbol{Q_1})^{-1}(\boldsymbol{I_n}\boldsymbol{Q_2} + \boldsymbol{M}). \tag{14}$$

Hence, the complete impedance model of PETT is given by

$$Z_t(f_p) = \dot{U}_p/\dot{I}_p = \boldsymbol{Z_{t(2,2)}} \tag{15}$$

where $\boldsymbol{Z_{t(2,2)}}$ represents the $(2,2)$th element of the matrix $\boldsymbol{Z_t}$.

When the DAB converter is viewed as a passive circuit [3], [4], the model of DAB converter can be expressed as

$$Z_{E\text{dab}}(s) = 1/(sC_2 + 1/R_L) + sL_r. \tag{16}$$

Then, the simplified PETT model is expressed as Z_{teq} by only replacing Z_{dab} with Z_{Edab}. Also, if another topology of dc–dc converter, e.g., *LLC* converter, is used in the PETT, the model can be established by a similar substitution.

III. Low-Frequency Stability Analysis of PETT

Based on the stability criterion of the cascade systems, the stability of the PETT-based train-grid system can be evaluated by the phase margin (PM), i.e.,

$$\text{PM} = 180^\circ - |\angle Z_g(j\omega_f) - \angle Z_{\text{PETT}}(j\omega_f)| \tag{17}$$

where Z_g is the traction grid impedance, ω_f is the frequency of magnitude intersection, and Z_{PETT} represents the impedance model of the PETT. Separately, Z_{PETT} is equal to Z_{teq} for the simplified PETT, and it is equal to Z_t for the complete PETT.

For the simplified PETT, taking the proportional gain of dc-link voltage control as an example, different values of k_{pvc} are traversed to identify the critical value of k_{pvc} at which the system becomes critically stable. Subsequently, the bode diagrams of traction grid and simplified PETT with the variation of k_{pvc} are depicted in Fig. 2. Observations from Fig. 2 suggest that, in the low-frequency range, the phase of traction grid remains 90°, while the phase of simplified PETT varies with different k_{pvc}. More specifically, with k_{pvc} being selected as 1.2, 1.5, and 1.9, the PM of simplified PETT system is calculated as 5.4°, 2.8°, and −0.4°, respectively. This represents the stability of system decreases with increasing k_{pvc}, in which the critical value is with $k_{pvc} = 1.9$. Similarly, to search the critical value of k_{pvc} for the complete PETT, Fig. 3 gives the bode diagrams of traction grid and complete PETT with different k_{pvc}. Obviously, the phase of the complete PETT also reduces with k_{pvc} increasing in the low-frequency region. However, as k_{pvc} increases to 1.1, the phase of the complete PETT at the frequency of magnitude intersection is about −90.3°, implying a PM of −0.3°. It can be viewed as a critical stabilization of the system with $k_{pvc} = 1.1$. Therefore, Figs. 2 and 3 express that the stability boundary of the PETT-based train-grid system is amplified when using

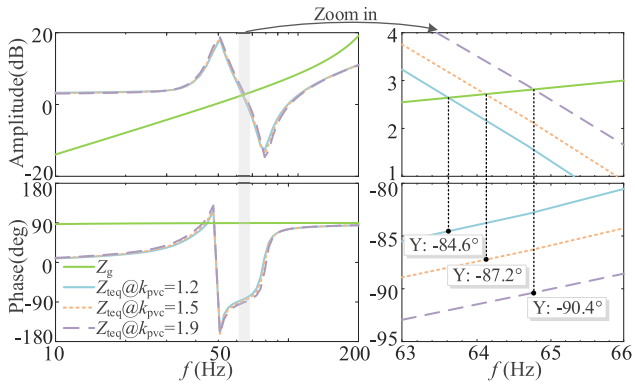

Fig. 2. Bode diagrams of simplified PETT with the variation of k_{pvc}.

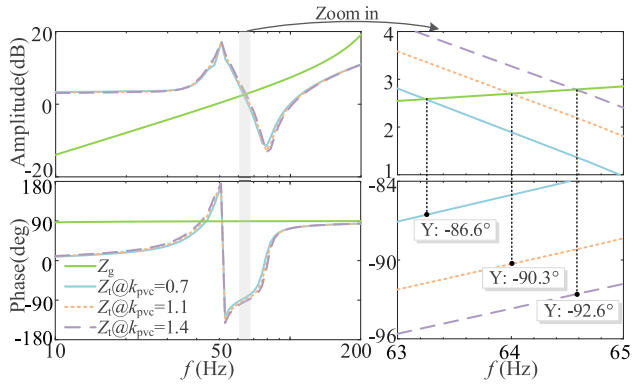

Fig. 3. Bode diagrams of complete PETT with the variation of k_{pvc}.

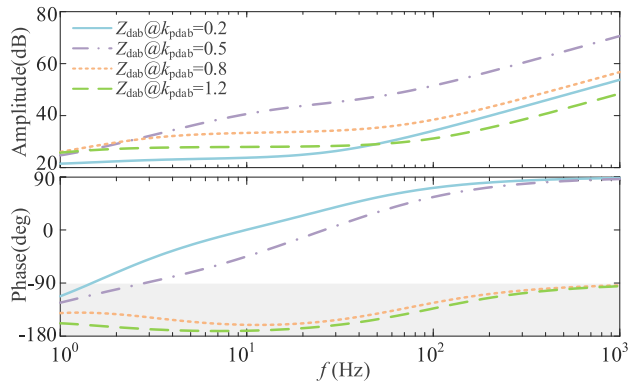

Fig. 4. Impedance characteristics of the DAB converter.

simplified PETT for stability analysis. For instance, when $k_{pvc} = 1.2$, the system is unstable with Z_t for stability analysis, but stable with Z_{teq} for stability analysis. That indicates that the DAB converter has a significant impact on the low-frequency stability of the PETT.

To further reveal the mechanism of the above outcome, the closed-loop impedance characteristics of the DAB converter are depicted in Fig. 4 with the variation of k_{pdab}. Fig. 4 shows that the phase of the DAB converter decreases with k_{pdab} increasing. Notice that when $k_{pdab} \geq 0.8$, the phase of the DAB converter

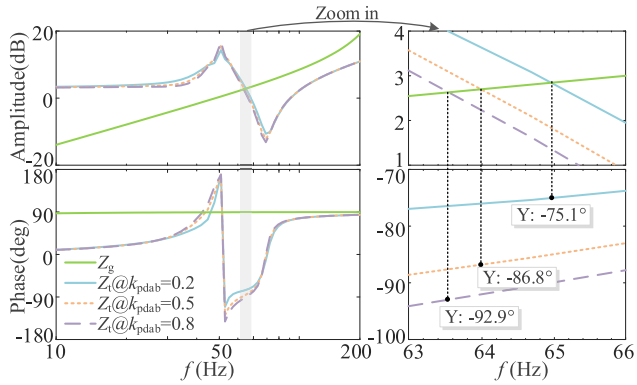

Fig. 5. Bode diagrams of complete PETT with the variation of k_{pdab}.

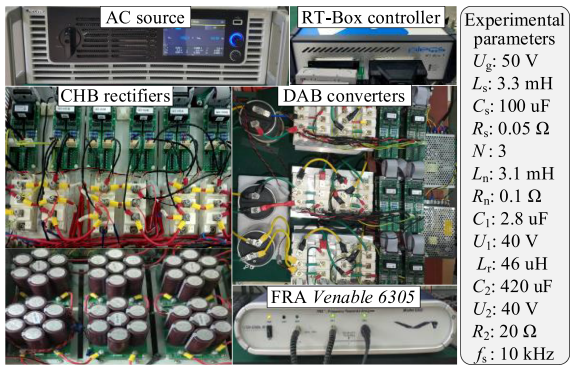

Fig. 6. Experimental setup and main circuit parameters of the PETT.

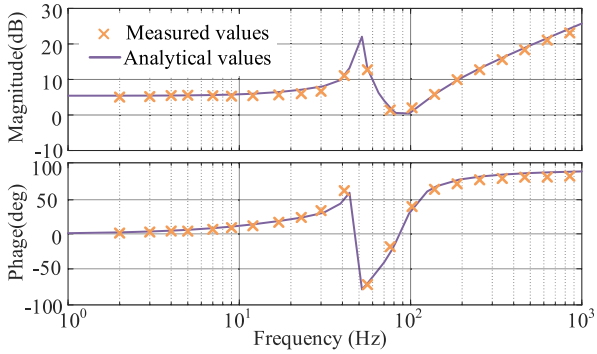

Fig. 7. Measured value and analytical one of the complete PETT impedance.

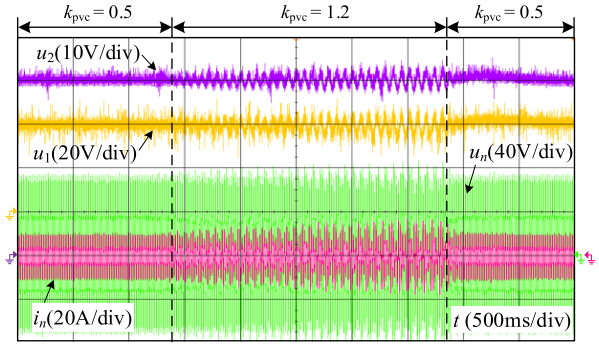

Fig. 8. Test results of the complete PETT with the variation of k_{pvc}.

is less than $-90°$ in a wide frequency range, exhibiting negative impedance characteristics. This will pose a challenge to the stability of the PETT-based train-gird system. To further illustrate this, the influence of k_{pdab} on the system is analyzed in Fig. 5. Also, Fig. 5 displays that the proportional gain of DAB converter affects the impedance of the complete PETT near the fundamental frequency. Then, a variation in k_{pdab} from 0.5 to 0.8 leads to a decrease in the phase of the PETT from $-86.8°$ to $-92.9°$. This represents that the PM of the PETT-based train-grid system is changed from positive to negative, implying that the system will be unstable.

Therefore, the above analysis has indicated that the negative damping features of the DAB converter push the phase of the overall PETT system into a negative damping region at the intersection frequency, resulting in the issue of the LFO and destabilization of the system. However, this effect cannot be found in a simplified topology because the simplified DAB converter is a passive circuit with always positive damping. Moreover, it can be concluded from Figs. 2 to 5 that the LFO of the PETT-based train-grid system is jointly affected by both the DAB converter and CHB rectifiers. Hence, when the active damping characteristic of the DAB converter is disregarded in stability analysis of the LFO, it may lead to the inaccurate analysis result.

IV. Experimental Validation

In order to verify the correctness of modeling and analysis, the experimental tests are conducted, where the setup of the PETT is exhibited in Fig. 6 with the main parameters attached. With the help of a frequency response analyzer *Venable 6305*, the measured results and the analytical results of the PETT impedance are plotted in Fig. 7. Based on the values given in Fig. 7, the measured impedance and the theoretical impedance demonstrate a high degree of consistency over a wide frequency range. This confirms the accuracy of harmonic linearization modeling for the PETT.

To clearly demonstrate the stability difference between complete PETT and simplified PETT, a special testing method is designed, presented in the Appendix. Accordingly, based on the complete PETT, the proportional gain of dc-link voltage controller is changed to verify the aforementioned analysis. In detail, when k_{pvc} is increased from 0.5 to 1.2, the test results from Fig. 8 illustrate that the dc-link voltage exhibits low-frequency fluctuations, and the ac-side voltage and current are oscillating and distorting. Obviously, the LFO occurs in the PETT system and the oscillation frequency is about 64 Hz. Then, the oscillation situation restores a steady state as k_{pvc} decreases, which implies that the stability is improved. With $k_{\mathrm{pvc}} = 1.2$, Fig. 9 displays the different test results for simplified PETT and complete PETT. More specifically, when using a simplified PETT, the test results manifest a stable state. However, as a complete PETT is operated, the dc-link voltage, the ac-side voltage, and the ac-side current express a characteristic of the LFO in Fig. 9. This means that the LFO occurs in the complete PETT but is not detected in the simplified topology, which

TABLE I
COMPARISON BETWEEN THE PROPOSED METHOD AND CURRENT STUDIES

Studies	Modeling of dc—dc converter	Control loop of ac—dc converter	Model order of PETT	Influence of dc—dc converter on stability	Oscillation mechanism	Accuracy of stability analysis
In [5]	Complete circuit	Only current loop	1×1	Neglected	Missing	Poor
In [4]	*RLC* equivalent	All considered	2×2	Neglected	Missing	Poor
In [3]	*RC* equivalent	All considered	2×2	Neglected	Analyzed	Normal
This letter	Complete circuit	All considered	1×1	Considered	Analyzed	Great

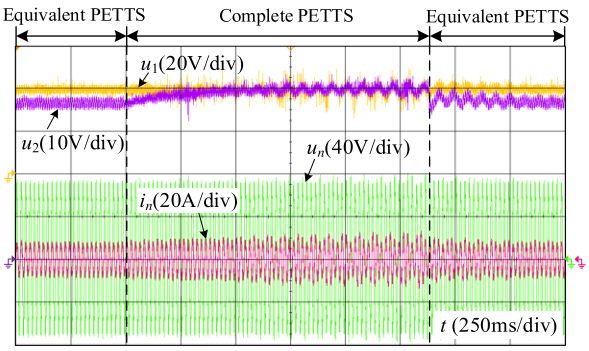

Fig. 9. Test comparison of simplified or complete PETT.

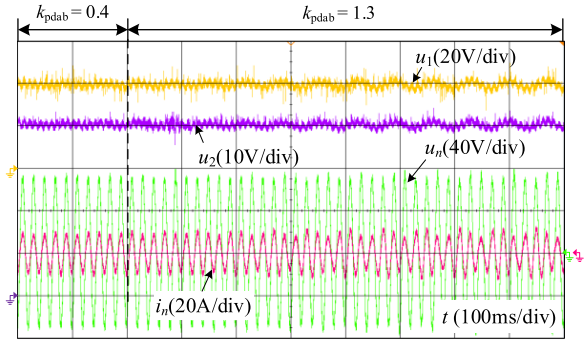

Fig. 10. Test results of the complete PETT with the variation of k_{pdab}.

confirms that the use of a simplified DAB model may lead to an unreliable analysis result in the PETT application.

In addition, Fig. 10 illustrates the effect of DAB converters' control gain on the stability of PETT when $k_{\text{pvc}} = 1.2$. It is observed that the system is stable with $k_{\text{pdab}} = 0.4$, whereas the feature of the LFO is exposed with $k_{\text{pdab}} = 1.3$. This suggests that a high value of k_{pdab} may lead to system oscillation. Furthermore, it can be concluded from Figs. 8–10 that the issue of the LFO in the PETT-based train-grid system is influenced by both the CHB rectifiers and the DAB converter, which aligns with the theoretical analysis.

A comprehensive comparison between the proposed analysis method and current research is provided in Table I. Observations from Table I show that the existing studies result in a limited accuracy of stability analysis due to equivalent modeling or incomplete stability analysis. In contrast, this letter that accounts for the influence of the dc–dc converter and undertakes a thorough stability analysis enables to provide a comprehensive understanding of the LFO in the PETT-based train-grid system. Consequently, it yields more satisfactory results in stability analysis.

V. CONCLUSION

This letter develops a novel perspective from a DAB converter to analyze the low-frequency stability of the PETT-based train-grid system, where the impact mechanism of DAB converter on the LFO is thoroughly revealed through the established harmonic linearization model. The analytical findings and experimental validations have indicated that the LFO of the PETT-based train-grid system is jointly affected by both the DAB converter and the CHB rectifiers, and the use of a simplified DAB converter will result in an imprecise analysis result. More thoroughly, the DAB converter with a high control gain exhibits negative damping characteristics, which push the overall system into a negative damping region. This narrows the stability margin of the PETT-based train-grid system and contributes to the issue of the LFO.

APPENDIX

The conversion coefficients $k_{m1}(s)$–$k_{m4}(s)$ are separately expressed as

$$\begin{aligned}
k_{m1}(s) &= H_{\text{cc}}(s)\left(H_{\alpha}(s_{+1}) + jH_{\beta}(s_{+1})\right) \\
&\quad + K_{\text{ou}}\left(H_{\beta}(s_{+1}) - jH_{\alpha}(s_{+1})\right) \\
k_{m2}(s) &= H_{\text{cc}}(s)\left(H_{\alpha}(s_{-1}) - jH_{\beta}(s_{-1})\right) \\
&\quad + K_{\text{ou}}\left(jH_{\alpha}(s_{-1}) + H_{\beta}(s_{-1})\right) \\
k_{m3}(s) &= H_{\text{cc}}(s)\left(H_{\beta}(s_{+1}) - jH_{\alpha}(s_{+1})\right) \\
&\quad - K_{\text{ou}}\left(H_{\alpha}(s_{+1}) + jH_{\beta}(s_{+1})\right) \\
k_{m4}(s) &= H_{\text{cc}}(s)\left(jH_{\alpha}(s_{-1}) + H_{\beta}(s_{-1})\right) \\
&\quad - K_{\text{ou}}\left(H_{\alpha}(s_{-1}) - jH_{\beta}(s_{-1})\right).
\end{aligned}$$

The transfer function matrices $\boldsymbol{Q_1}$ and $\boldsymbol{Q_2}$ are given by

$$\boldsymbol{Q_1} = \frac{1}{2}\begin{bmatrix} 0 & H_{\text{co}}(s_{+1}) & 0 \\ H_{\text{co}}(s_{-2}) & 0 & H_{\text{co}}(s_{+2}) \\ 0 & H_{\text{co}}(s_{-1}) & 0 \end{bmatrix},$$

$$\boldsymbol{Q_2} = \frac{1}{2}\begin{bmatrix} k_i(s_{-1}) & 0 & 0 \\ 0 & k_i(s) & 0 \\ 0 & 0 & k_i(s_{+1}) \end{bmatrix}$$

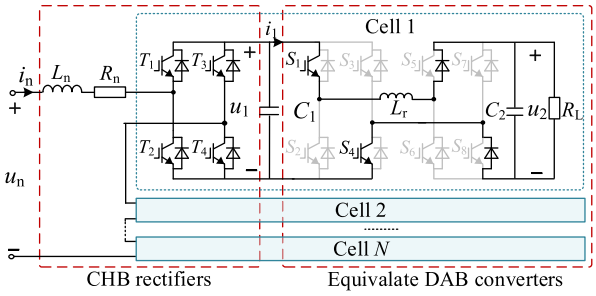

Fig. 11. Simplified PETT topology used for experimental testing.

where $k_i(s) = k_{m1}(s_{-1}) - jk_{m3}(s_{-1}) + k_{m2}(s_{+1}) + jk_{m4}(s_{+1})$.

To intuitively make the stability comparison between complete and simplified PETT, a special testing method is given. In this method, the switches of the DAB converter are reused, including two states. For the first switching state, all switches of the DAB converter are triggered by normal control signals, effectively representing the entire PETT circuit. For another switching state, when only two switches S_1 and S_4 of the DAB converters are turned on and others are turned off, this configuration without an isolation transformer is shown in Fig. 11. Seen from Fig. 11, the dc–dc converters are regarded as *LCR* circuit, which is regarded as the simplified PETT. Hence, by multiplexing the switches, the PETT can be simply tested between complete and simplified topology.

REFERENCES

[1] J. Feng, W. Q. Chu, Z. Zhang, and Z. Q. Zhu, "Power electronic transformer-based railway traction systems: Challenges and opportunities," *IEEE J. Emerg. Sel. Topics Power Electron.*, vol. 5, no. 3, pp. 1237–1253, Sep. 2017.

[2] D. Xie, C. Lin, H. Lin, W. Liu, Y. Du, and T. Basler, "OC switch fault diagnosis, pre- and postfault DC voltage balancing control for a CHBMC using SVM concept," *IEEE Trans. Power Electron.*, vol. 39, no. 1, pp. 677–692, Jan. 2024.

[3] Y. Hong, Y. Li, Z. Shuai, and H. Yang, "Modeling and low-frequency stability analysis of power electronic traction transformer-based train-network system," *CSEE J. Power Energy Syst.*, to be published, doi: 10.17775/CSEEJPES.2021.05000.

[4] C. Lin, "Modeling and harmonic instability analysis of the PET-based train-grid system," in *Proc. IEEE Energy Convers. Congr. Expo.*, 2022, pp. 1–7.

[5] Z. Wang, X. Yin, Y. Chen, and J. Lai, "Stability analysis and control for power electronic transformer with FRT capability," *Int. J. Elect. Power Energy Syst.*, vol. 140, pp. 107956–107967, Sep. 2022.

[6] C. Gu, Z. Zheng, L. Xu, K. Wang, and Y. Li, "Modeling and control of a multiport power electronic transformer (PET) for electric traction applications," *IEEE Trans. Power Electron.*, vol. 31, no. 2, pp. 915–927, Feb. 2016.

[7] H. Lin, C. Cai, J. Chen, Y. Gao, S. Vazquez, and Y. Li, "Modulation and control independent dead-zone compensation for H-bridge converters: A simplified digital logic scheme," *IEEE Trans. Ind. Electron.*, to be published, doi: 10.1109/TIE.2024.3370975.